35th Annual International Conference of the IEEE EMBS
Osaka, Japan, 3 - 7 July, 2013

A synchronization method for wireless acquisition systems, application to brain computer interfaces

M. Foerster, S. Bonnet, A. van Langhenhove, J. Porcherot, G. Charvet

***Abstract*—A synchronization method for wireless acquisition systems has been developed and implemented on a wireless ECoG recording implant and on a wireless EEG recording helmet. The presented algorithm and hardware implementation allow the precise synchronization of several data streams from several sensor nodes for applications where timing is critical like in event-related potential (ERP) studies. The proposed method has been successfully applied to obtain visual evoked potentials and compared with a reference biosignal amplifier. The control over the exact sampling frequency allows reducing synchronization errors that will otherwise accumulate during a recording. The method is scalable to several sensor nodes communicating with a shared base station.**

I. Introduction

In many biomedical applications, it is mandatory to collect data from several wireless sensors in a synchronized way. One of these time-critical applications may concern the recording of the electrical brain activity from a wireless EEG/ECoG system. These recording methods are well known for the good temporal resolution they offer. In neurosciences, time issues are particularly relevant when event-related potentials (ERPs) are measured. Indeed these potentials are time-locked with a presentation stimulus (visual, acoustic or somesthetic). Since the amplitude of these potentials is very low, in the range of few µV, with a low signal to noise ratio, it is often necessary to average several repetitions to correctly visualize the ERP. The ERP is further analyzed in terms of latency and amplitude and several medical indications can be made from it. Another field of application relates to brain-computer interface (BCI) systems. EEG-based P300 spellers have recently been proposed in order for a motor-disabled patient to spell a word by focusing his attention on a target character [1]. A grid of 6x6 characters is flashed randomly along its columns and its rows. When the target character is highlighted, this will produce a typical brain response with a positive deflection 300ms after flash onset. Timing issues (offsets, drifts) are critical in this type of application since such paradigm can last for a long period of time without being reset.

On tethered devices, the measurable trigger signal of these stimuli is usually recorded on the same device that records the biosignals, hence discarding the need for a synchronization method. Recently, wireless EEG/ECoG recording devices have been described in the literature [2][3][4] and are being more and more used due to the intrinsic advantages they offer. For these devices, a solution must be found to synchronize in a proper way both data streams of stimuli and biosignals. A simple but effective solution is described in this paper. This paper illustrates how the proposed method has been applied to one such wireless implant with an external stimulation unit and validated by recording wirelessly a visual evoked potential.

This project received financial support through grants from the French National Research Agency (ANR-Carnot Institute), Fondation Motrice, Fondation Nanosciences, Fondation de l'Avenir, Région Rhône-Alpes and Fondation Philanthropique Edmond J Safra.

M. Foerster, G. Charvet are with CEA/LETI/CLINATEC, Minatec Campus, Grenoble, France (contact: michael.foerster@cea.fr)

S. Bonnet, A. van Langhenhove, J. Porcherot, are with CEA/LETI/DTBS, Minatec Campus, Grenoble, France.

II. Methods

A. System overview

The synchronization algorithm detailed in this paper has been applied to the ECoG recording implant described in [5]. The simplified architecture of the WIMAGINE® implant is depicted in Figure 1. : 64 electrodes are interfaced with two ASICs which amplify and digitize the electrical activity of the brain. The raw acquired data is extracted by an MSP430 microcontroller and sent to a base station connected to a PC through a wireless connection using a low-power transceiver Zarlink ZL70102 in the MICS band (402–405MHz). The implant is powered remotely through an inductive link at 13.56MHz on which a very simple RFID-like communication link has been implemented. The base station can communicate with up to two implants and also acts as a recording device as it can record up to 8 analog or 16 digital signals. In a standard ERP protocol, the PC will therefore receive 3 different data streams: one from each implant and one from the stimulation unit.

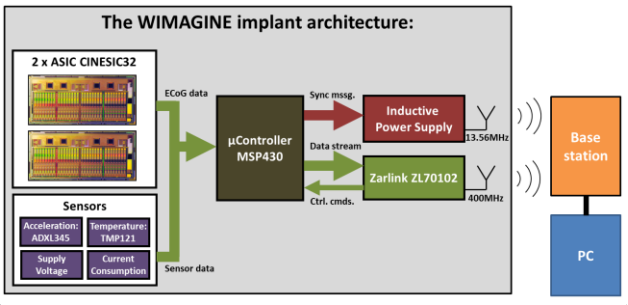

Figure 1. Simplified architecture of the WIMAGINE® implant

B. Principle of operation

The principle of the method presented here lies in the separation of the information sent from a source node S (in our case, one implant) to a target node R (the base station): one communication channel (the data link) will transmit the values of every EEG/ECoG sample while a second communication channel (the sync link) will transmit the temporal information. There are no particular requirements on the data link except that the loss of samples is identified.

On the contrary, the sync link has to guarantee a constant latency of the transmitted information but has no particular requirement in terms of data integrity or throughput.

Most commercial communication links similar to Bluetooth or Zigbee guarantee high data reliability on application level, meaning that several error correction and retransmission schemes take place in the low level MAC (Media Access Controller), which makes the latency of each transmitted packet dependent on the RF link quality. On the target node, a sample transmitted by this kind of link can therefore not be placed on a timeline with a higher accuracy than the latency jitter. Furthermore, data streams from multiple source nodes cannot be placed on a common timeline with precision.

For the WIMAGINE® platform, the data of each implant is sent on the Zarlink channel and each sample is prefixed with a header containing a 16-bit value increased for each sample called timestamp; this will allow the identification of lost packets. The synchronization messages are sent by simply load modulating the Manchester code of a synchronization word on the inductive link.

The ROBIK platform [2] is very similar to the former, except that the inductive link is now replaced by a battery. Here, the synchronization messages are sent through a rudimentary IR link using a Vishay TFDU4101 [6]. Each time the IR component of the base station side receives an IR message, an interrupt is generated on the microcontroller it is connected to. The microcontroller reads the received message and sends a pulse to the I/O interface of the terminal. Both applications, illustrated in Figure 2. , use a synchronization link that is cheap, simple, not particularly robust but that has a controlled latency.

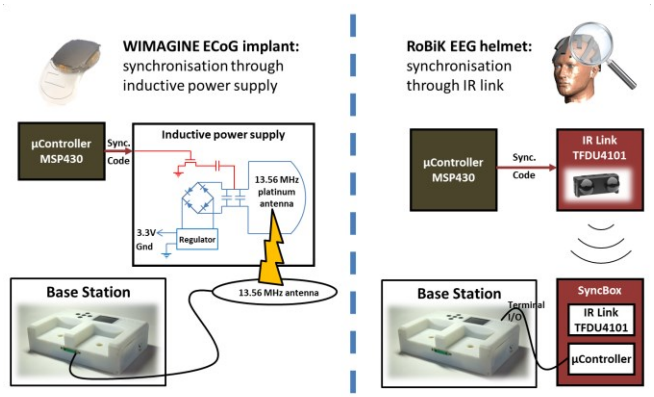

Figure 2. Implementation of the synchronisation link on the WIMAGINE® [3] and ROBIK [2] platforms.

C. Algorithm

In addition to the data, the source node S sends periodically (over the synchronization link) a series of synchronization messages to the target node R every m recorded values. The nth message is sent at time T_n of S's clock and received at time R_n of R's clock. The sync message delay δ is supposed to be constant and known from a calibration procedure. To guarantee δ is constant, a specific channel must be used (infrared channel for instance), uncorrelated from the data acquisition channel.

The algorithm proceeds by first estimating the offset between the different devices (here one implant and one stimulation unit). Denote $t_0^{(STIM)}$ the time of the first stimulation unit sample acquired in R's clock. Every time a new sync message is received at R_n $(n \geq 0)$, the time offset between both devices is given by

$$\Delta[n] = R_n - \delta - mn\bar{T}_e^{(IM)} - t_0^{(STIM)} \qquad (1)$$

with $\bar{T}_e^{(IM)}$ being the theoretical sampling rate of the source node S. Between 2 sync messages received respectively at R_{n_1} and R_{n_2}, the data samples will be positioned at:

$$t_{mn_1+k} = R_{n_1} + k\bar{T}_e^{(IM)} - \Delta[n_1];\ 0 \leq k < m(n_2 - n_1) \qquad (2)$$

Note that offset is recalculated every time a new synchronization message arrives in order to limit the impact of sync message jitter and also take into consideration drift between implants and base station clocks. The system is robust to synchronization messages loss since the approximate time of reception of a synchronization message is known.

In addition, the real sampling rate of the implant can be estimated. Suppose that the first sync message has been received at R_{n_0} ($n_0 \geq 0$). Then every time a new sync message is received at R_n ($n > n_0$), one can estimate the S's sampling rate as:

$$T_e^{(IM)}[n] = \frac{R_n - R_{n_0}}{m(n-n_0)};\quad n > n_0 \qquad (3)$$

This sampling rate is generally different from the theoretical one, as expressed by the ratio $\eta[n] = T_e^{(IM)}[n]/\bar{T}_e^{(IM)}$. This drift correction is particularly important when low-grade quartz crystals are used or if experiments last for several hours without any reset. The frequency accuracy of quartz crystals used for timing the CPUs of microcontrollers is in the order of 10's of parts per million (ppm). Importantly, once the drift has been estimated, it is possible to accurately locate the data samples on the R's clock by using this improved value, just by replacing $\bar{T}_e^{(IM)}$ by $T_e^{(IM)}[n_1]$ in Eq. (2). This drift correction is important for synchronization messages sent at low frequencies.

Once offset and drift have been estimated, it is possible to align all data streams on the same timeline and resample it to a sampling frequency $T_e^{(ACQ)}$. The highest device's sampling rate is usually chosen as it guarantees that no point of measurement is lost, only channels from devices running at a lower frequency than $T_e^{(ACQ)}$ will have some NaN values reported. We assign each measurement point to one unique data point – the nearest in time – in the resampled data stream. Note that these NaN values can be replaced later by interpolation. A FIFO of samples is set up to deal with timing constraints when synchronization is done online: the system can then wait for the data from all inputs (implants and stimulus acquisition system) to be received before doing any data processing on the merged data stream.

III. RESULTS

A. Calibration procedure

The synchronization method is first validated with a square pulse generator connected both to the input channel of two RF implants and to the acquisition unit in the base station, as shown in Figure 3. Both implant acquisitions are started separately and will therefore not have the same t_0. The synchronization method is applied online to this dataset with a null sync message delay. The method is able to correct for offset and drift but will not be able to compensate for systematic sync message delay. Hence, the lag between each sensor node and the acquisition unit in the base used as reference will give the synchronization message delay δ.

More precisely, for a given sensor node, the residual delay δ[k] is estimated by computing, for the k^{th} square pulse, the inter-correlation function between the implant signal and the pulse generator signal. The lag with maximal correlation is defined to be the estimated sync message delay.

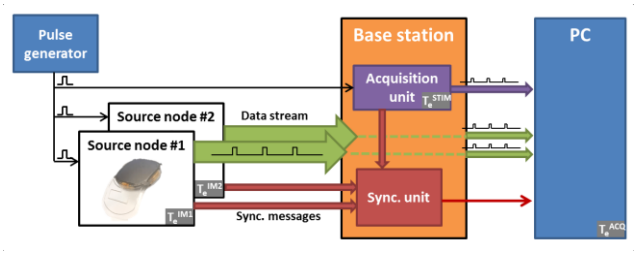

Figure 3. Calibration procedure

One is then able to compute the probability density function of the random variable δ for the RF implant and thus estimate its mean and its standard deviation. At the end of the calibration procedure, the sync message delay is set to the median of the distribution. Note that the precision of the estimation is limited by the highest sampling frequency of the three data streams. Figure 4. presents the delay between the rising edges of one implant and the terminal. This delay includes the transmission latency of the synchronization message, but also the internal constant delays due to filtering and buffering, as well as some random delays [7].

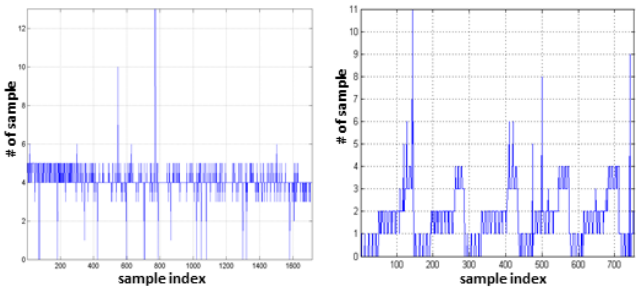

Figure 4. Lag (in samples) between sensor node #1 signal and reference pulse signal. Left: with frequent drift correction. Right: with less frequent drift correction. Note the increasing drift between two synchronisation messages.

In this calibration setup, sync messages are sent every 4,096 samples (~4s) by each implant. The delay between the rising edges of the signals returned from the implants and the terminal is measured to be 4.1ms, with a low dispersion, as expected. The ratio $\eta[n] = T_e^{(IM)}[n]/\overline{T}_e^{(IM)}$ is measured and corresponds to a drift of -32ppm for implant #1 and -33ppm for implant #2. These values are in good accordance with the datasheet of the quartz crystal used in the implant, the C-MAC CFPS-69IB given at 50ppm [8].

When sync messages are sent too rarely, one can observe that drift correction (eq. 3) is mandatory with this method to prevent local drifts of the different data stream. This can be seen in Figure 4. where a periodical reset of the delay $\delta[k]$ is observed every 4s in case of no drift correction. Here sync messages are sent every 2^{17} data points (~134s @ 976Hz), thus approximately every 134 pulses for a 1Hz square pulse generator.

B. Visual evoked potentials

Visual evoked potentials (VEPs) provide means of investigating functional disturbances in the afferent pathway being stimulated. Moreover, they are used to monitor patients and are an aid in diagnosis. Indeed, VEPs provide useful information when patients do not have clean evidence of visual dysfunction on clinical examination [9] [10].

As one of the main issues with VEPs is the synchronization between the synchronization between the stimulus signal and the EEG/ECoG signal, the proposed synchronization method is tested in EEG to form a visual evoked potential (VEP). The set-up is described in Figure 5.

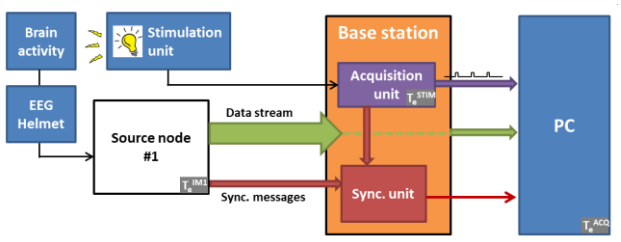

Figure 5. Set-up for the VEP experiment

One male (age 30) participated in this experiment and a LED stimulator was used to elicit the VEPs. This stimulator generates flashes of 10ms duration every 0.5s.

The EEG signals were recorded from PO7, PO3, POz, PO4, PO8, O1, Oz, O2 locations of the international 10-20 system depicted in Figure 6. Those signals were referenced against AFz and the ground electrode was placed on Cz. The EEG signals were acquired with two different recording systems in two successive acquisitions. The first recording was made with a WIMAGINE® implant connected to an EEG headset and communicating with a base station. The second recording was made with a g.USBamp amplifier from g.tec [11]. For each recording, the test subject was submitted to 128 visual stimuli.

For the WIMAGINE® acquisitions, the EEG signals were sampled at 976.563Hz with a bandwidth of 0.5Hz–300Hz and the trigger signal was sampled at 800Hz. A notch filter centred at 50Hz was also applied. The EEG signals from implant and trigger from terminal were synchronised using the presented method with synchronization messages sent every 4096 frames. The system operated drift correction based on the device's synchronization messages. For the g.USBamp, signals and trigger were sampled at the same

time with a sampling rate of 1200Hz and a bandwidth of 0.5Hz-250Hz. A notch filter inside the system removes the 50Hz power line noise.

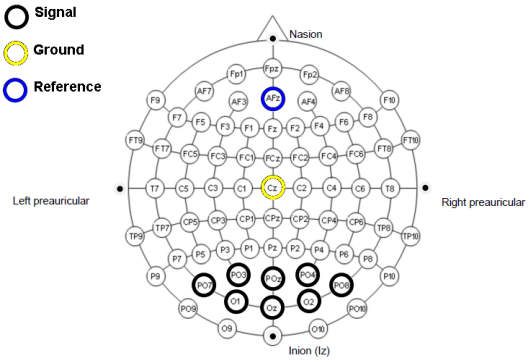

Figure 6. EEG electrodes locations for both VEP recordings.

To compute the VEP, EEG signals were band pass filtered between 1Hz and 40Hz. After the beginning of each flash, a window of 300ms was extracted. Finally, the 128 extracted windows were averaged. Figure 7. depicts the VEP extracted in Oz for each recording. As we can see, the main components (N1, P1, N2, P2, N3, P3) of the VEP appear at the same latencies in both the WIMAGINE® recording and on the g.USBamp recording. The differences observed in the amplitudes of both signal could be related to the fact that both recordings were not performed simultaneously. This comparison shows that the synchronization method removes the wireless induced latencies, provides sufficient accuracy for performing wireless VEP and is stable over time.

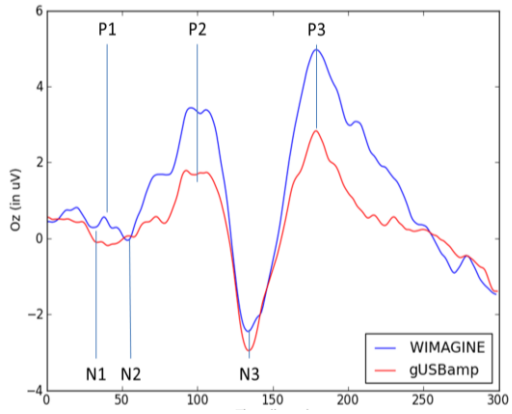

Figure 7. Visual evoked potentials obtained with the WIMAGINE® and g.USBamp systems.

IV. Discussion

In the different setups presented in this paper the period of synchronization messages sent from the source nodes to the target node was in the order of 4 seconds. This frequency could be optimized by taking into account the sampling frequency of the source node, the maximum drift of the source node's clock and the requested precision of the synchronized data streams. Cognitive evoked potentials like P300, requiring less precision than visual evoked potentials, could be acquired with synchronization messages sent every few minutes. The proposed method will thus be well adapted for P300-based speller on wireless BCI systems.

V. Conclusion

A method for performing a precise synchronization of wireless acquisition systems was proposed and evaluated. The method was implemented on a wireless ECoG recording implant and on a wireless EEG recording headset. Two physical implementations of the synchronization link have been described but the synchronization procedure described here can be performed with other links respecting the listed requirements. A calibration method was introduced for measuring the delay of the synchronization message and visual evoked potentials could be successfully recorded using the presented method and algorithm.

Acknowledgment

This work was performed thanks to the close collaboration of the technical staff of CEA/LETI/DTBS and CEA/LETI/CLINATEC®. The authors wish particularly to thank S. Filipe and G. Chatalic for their involvement in the ROBIK project and in the development of the IR link.

References

[1] B. Rivet, A. Souloumiac, V. Attina, and G. Gibert, "xDAWN algorithm to enhance evoked potentials: Application to Brain-Computer Interface", *IEEE Trans. Biomed. Eng.*, vol. 56(8), pp. 742-750,

[2] S. Filipe, G. Charvet, M. Foerster et al., "A wireless multichannel EEG recording platform," presented at the *Engineering in Medicine and Biology Society, EMBC 2011,* pp. 6319-6322, Aug. 30 2011-Sept. 3 2011

[3] G. Charvet, F. Sauter, M. Foerster, et al., "WIMAGINE: Long-term wireless 64-channel ECoG recording implant for clinical applications", presented at the *Engineering in Medicine and Biology Society, EMBC 2013* (submitted)

[4] Y. Ming, D.A. Borton, J. Aceros, et al., "A 100-channel hermetically sealed implantable device for wireless neurosensing applications" *International Symposium on Circuits and Systems, ISCAS 2012*, pp. 2629-2632, 20-23 May 2012

[5] M. Foerster, J. Porcherot, S. Bonnetet al., "Integration of a state of the art ECoG recording ASIC into a fully implantable electronic environment", presented at the *Biomedical Circuits and Systems Conference, (BioCAS) 2012*

[6] Datasheet of the Vishay TFDU4101 available at http://www.vishay.com/docs/81288/tfdu4101.pdf

[7] C. Beck, J. Nagel, P. Hevesi, G. Bretthauer, "RTS-MAC: A Relative Time Synchronization MAC Protocol for Low Duty Cycle Body Sensor Networks," *International Journal of Wireless Information Networks*, vol. 19, pp. 163–172, 2012.

[8] Datasheet of the C-MAC CFPS-69IB available at http://www.farnell.com/datasheets/57061.pdf

[9] M. J. Aminoff, D. S. Goodin, "Visual evoked potentials", *Journal of Clinical Neurophysiology*, vol. 11, issue 5, pp. 493-499, 1994.

[10] J. V. Odom, M. Bach, C. Barberet al., "Visual evoked potentials standard (2004)", *Documenta Ophthalmologica*, vol. 108, issue 2, pp. 115-123, March 2004.

[11] g.Tec, g.USBamp recording system, available: http://www.gtec.at/Products/Hardware-and-Accessories/g.USBamp-Specs-Features